Stuck on an island: land area changes during Holocene sea-level rise and implications for species evolution

Author: Yanxi Shi

Department: Faculty of Geosciences, Utrecht University, Utrecht, the Netherlands

Supervisor(s): Jaap Nienhuis[1], Kenneth Rijkdijk[2]

Co-contributor: Johannes De Groeve[2]

Date of Submission: 22/04/2024

[1] Coastal Dynamics and Fluvial System, Faculty of Geosciences, Utrecht University, Utrecht, the Netherlands

[2] Institute for Biodiversity and Ecosystem Dynamics, Faculty of Science, University of Amsterdam, Amsterdam, the Netherlands

Contents

Abstract

Global biogeographic models are essential for reconstructing paleo-environments and understanding species evolution and modern biodiversity. Present state-of-the-art models include the effects of sea-level rise and isostasy on Holocene biogeography but so far do not take sediment deposition and erosion into account. This could be a major issue near river deltas, where pronounced morphologic change due to high fluvial sediment fluxes has large potential effects on reconstruction of the past coastline positions.

Here we attempt to address this knowledge gap by using sediment cores to reconstruct the Holocene evolution of the Vietnamese Mekong Delta (VMD) from 11 ka BP to the present. For each time slice on a gridded surface, we calculate terrestrial and marine sedimentation rates and include this dynamic topography in a novel numerical paleo-coastline model. Model results simulate delta formation and its dynamic evolution during the Holocene period and show important consequences of the past wetland extent and connections between fresh-water environments. The period of 11-7 ka BP marked a significant retreat of coastlines and expansion of shelf areas followed by a relative temporary equilibrium in landmass change for the next 3 kyr. The latest phase from 4 ka BP to the present indicated a regression phase, where the coastline notably progradated seawards, shaping the modern landscape.

1. Introduction

Sea-level change, reflecting broader shifts in climate, significantly influences deltaic evolution and it also plays a vital role in shaping the current biodiversity and evolutionary situation of both marine and terrestrial realms (Nienhuis et al., 2022; De Groeve et al., 2022). While sea-level rise plays a significant role, it is not the sole driver of the delta's morphodynamical evolution. River sediment discharge collectively influences deltaic transformation (Tamura et al., 2012; Nienhuis et al., 2022).

1.1 Study area and its sedimentation condition

Deltas are typically landforms characterized by a positive sediment balance, advancing into the open sea. The main reason why the Vietnamese Mekong Delta is chosen to be the area to resolve this knowledge gap is because the Mekong River is one of the largest rivers in the world in terms of water discharge and sediment discharge, which would generate a dynamic deposition system (Ta et al., 2002; Tanabe et al., 2003). Recent seismic studies have shown that the Mekong River has formed deposits up to 15 m thick onshore, but the delta surface remains low-elevated, with gradients ranging from approximately 1 m/km to 1 cm/km (Minderhoud et al., 2022). Even most of the sediment would be deposited onshore, sediment deposits could extend seawards 8–10 km into the Gulf of Thailand, reaching water depths of up to 25 m (Liu et al., 2017).

Sediment on the delta is primarily deposited by the river and, to a lesser extent, from offshore sources along the coast (Nguyen et al.,2023). The Mekong River originates from the elevated Qinghai-Tibet Plateau, and flows through six nations—China, Myanmar, Laos, Thailand, Cambodia, and Vietnam, before it discharges into the South China Sea in the southern part of Vietnam (Li et al., 2018). The upper Mekong River's catchment sedimentation reaches are mainly influenced by tectonic uplift, particularly from the rising Himalaya massif. Tectonic uplift increases erosion rates of riverbank in the highlands, supplying more sediment to the fluvial system. As the Mekong River carries these sediments downstream, a significant portion will be deposited in the delta (Milliman and Syvitski,1992; Schimanski and Stattegger, 2004; Carling, 2009).

Other factor which controls sediment discharge appear to have secondary importance. A high sediment yield caused by abundant monsoonal precipitation and runoff along the riverside has resulted in distinct stratigraphic successions and sediment contribution to the development of a huge delta plain (Nguyen et al., 2010).

1.2 Sea-level change

Sea-level change during the post-glacial Holocene period has played a dominant role in the transformation of river-mouth coastal systems of the Mekong Delta from the estuary to the delta nowadays (Nguyen et al., 2010).

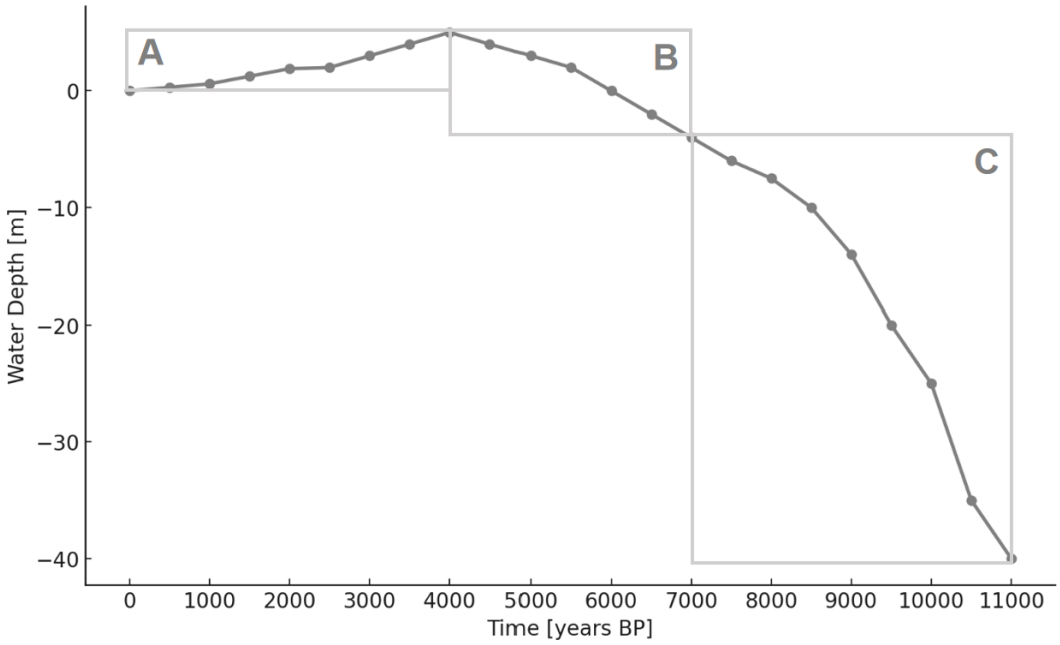

Fig.1. Reconstruction of sea-level changes for the Holocene period showing on Sunda region (Fig.2) where the VMD is located. Three main phases of sea levels which affect the shape of the VMD are Rapid Raising Phase (Phase C), Intermediate Deceleration Phase (Phase B) and Later Lowering Phase (Phase A). Water depth data compiled from Geyh et al., 1979, Sathiamurthy and Voris, 2006 and Hanebuth et al.,2010.

During the Last Glacial Maximum (LGM) period (26-20 ka BP), global sea levels dropped to the lowest position, more than 125 m below the present mean sea level (Hanebuth et al., 2010; De Groeve et al., 2022). The sea-level curve of the VMD

during Holocene can be divided into 3 phases (Fig.1): Rapid Raising Phase (Phase C), Intermediate Deceleration Phase (Phase B), and Later Lowering Phase (Phase A).

During 11-7 ka BP (Phase C), the Mekong Delta area experienced a long varying rapid sea-level rise, with the rates of 10-15m/ ka, because of deglaciation caused by global warming at the end of the LGM. There was a small pulse around 8.5 ka. Water depth was elevated from 40 m to 5 m compared to present-day mean sea level.

Phase B (7-4 ka BP) was characterized by relative deceleration of sea-level rise after previous phase, and reaching historical high stand of sea level, approximately 2 m or even more above modern sea level (Li et al., 2010).

A final sea level slow lowering from the high stand happened during Phase A (4 ka BP -present). This phase continues up until the present.

1.3 Biodiversity

The Mekong River ranks as the second-most biodiverse area in the world (Milliman and Syvitski,1992; Ishii et al.,2021). Due to the Mekong River system feeding a vast network of streams, rivers, and wetlands, it facilitates a range of aquatic habitats. Besides, the tropical climate and abundant rainfall support a diverse range of terrestrial species. The delta is rich in marshes and mangroves in the intertidal zone near the coastlines, swamp forests and associated shrubs in the wetland, and forests in the river drainage basin (Nguyen et al., 1998; Li et al., 2010; Hanebuth et al., 2010).

The diversification and migration in terrestrial and freshwater communities as well as intertidal and marine communities are strongly influenced by the historical relative position of the shoreline based on the dynamic process of transgression and regression during the Holocene (Hofreiter and Stewart, 2009; Woodruff and Turner, 2009; Woodruff, 2010; Li et al., 2012; De Groeve et al., 2022). The Mekong Delta landmass dynamics might have influenced the timing of the disappearance of the

gateway between the Mekong Delta and other lands on Sunda Shelf[3] (Sathiamurthy and Voris, 2006).

During the LGM, while the sea level was more than −125 m lower than today, it illustrates the maximum potential existence in terms of exposed land as biogeographic crossroad connecting Borneo and the nearby area (As shown in Fig.2). The existence of the exposed land facilitated the migration of both human populations and fauna across the region but became a barrier for marine biota's connection underneath the ocean (Hanebuth et al., 2010; De Groeve et al., 2022). The river and the surrounding coastal areas served as a habitat for various marine species temporarily, where they can live, reproduce, and get fed in order to survive.

However, the evolution of the delta landscapes might alter the shape of the lands and impact the connectivity of the species in later stages.

[3] Sunda Shelf is located in Southeast Asia. It includes islands of Borneo, Java and Sumatra and the bulk of the shelf forms the shallow seabed of the South China Sea, the coastal areas of Cambodia, Peninsular Malaysia, Singapore, Borneo, and parts of the coast of Indonesia, Thailand, and Vietnam. The VMD is closely connected to it. (Hanebuth et al.,2010).

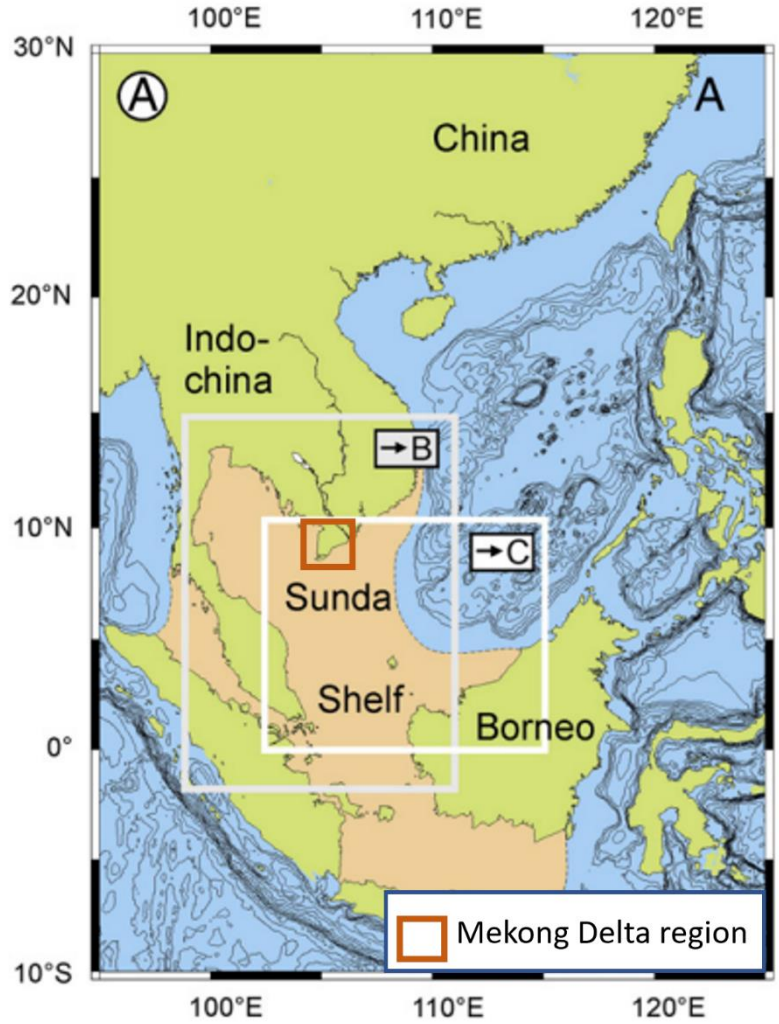

Fig.2. The Sunda Shelf approximate extent (orange) of subaerial exposure during the LGM period and the general location of the VMD in the Sunda Shelf (Source: Hanebuth et al., 2010).

To understand the biogeographic effect on the exposure and disappearance of the gateway, it is important to study how the Mekong Delta evolved during the Holocene, and assessing how its dynamics affected paleo-coastlines.

Many studies reconstruct paleo-coastlines by relating present-day seafloor depth directly to a past eustatic sea-level position. But at present, these models do not consider sediment deposition factors in their paleo-coastline reconstructions. This might yield some inaccuracies of the rates of coastline retreats, shelf expansions and land losses without taking these factors into account (De Groeve et al., 2022).

This thesis aims to develop and validate a model which is based on sea-level rise but adds delta sedimentation characteristics to reconstruct paleo-coastline movements in the Mekong Delta of past times.

2.Method

In this study, we have established a workflow (Fig. 3c) that allows us to reconstruct sedimentation from sediment cores and use it in a paleo-coastline model.

The workflow is initiated by refining the geographical boundary (study area) by using geomorphological criteria to focus on delta-affected areas. Extracting data on drilling cores from both onshore and offshore sources is required, followed by collecting and compiling to calculate sedimentation rates. These rates are then temporally interpolated to calculate cumulative sediment deposition thickness, in the meantime, the spatial numerical interpolation technique is applied to estimate sedimentation rates across the whole study area. In the end, the interpolated data is incorporated into a paleo-coastline model to generate a series of landmass maps spanning from 11 kyr BP to the present.

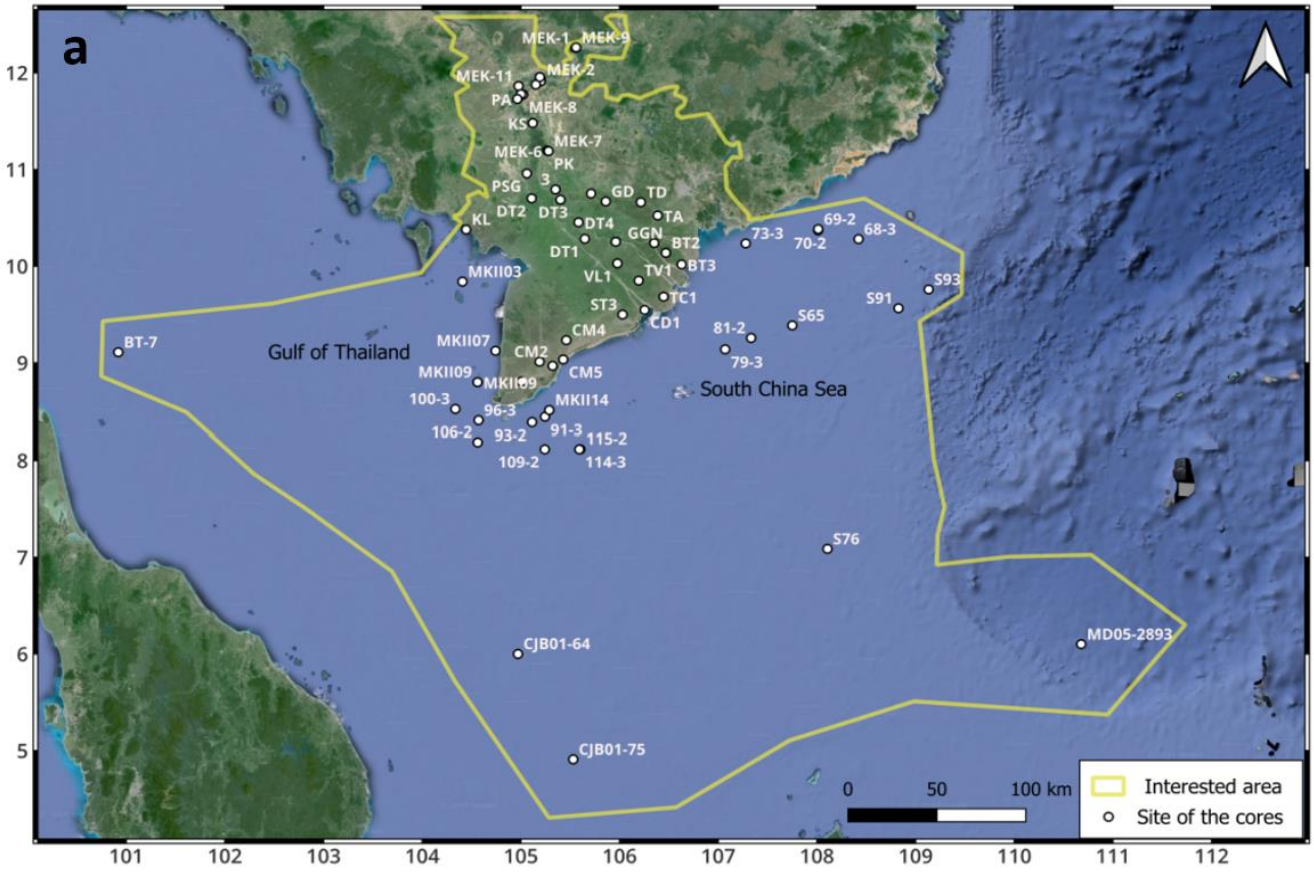

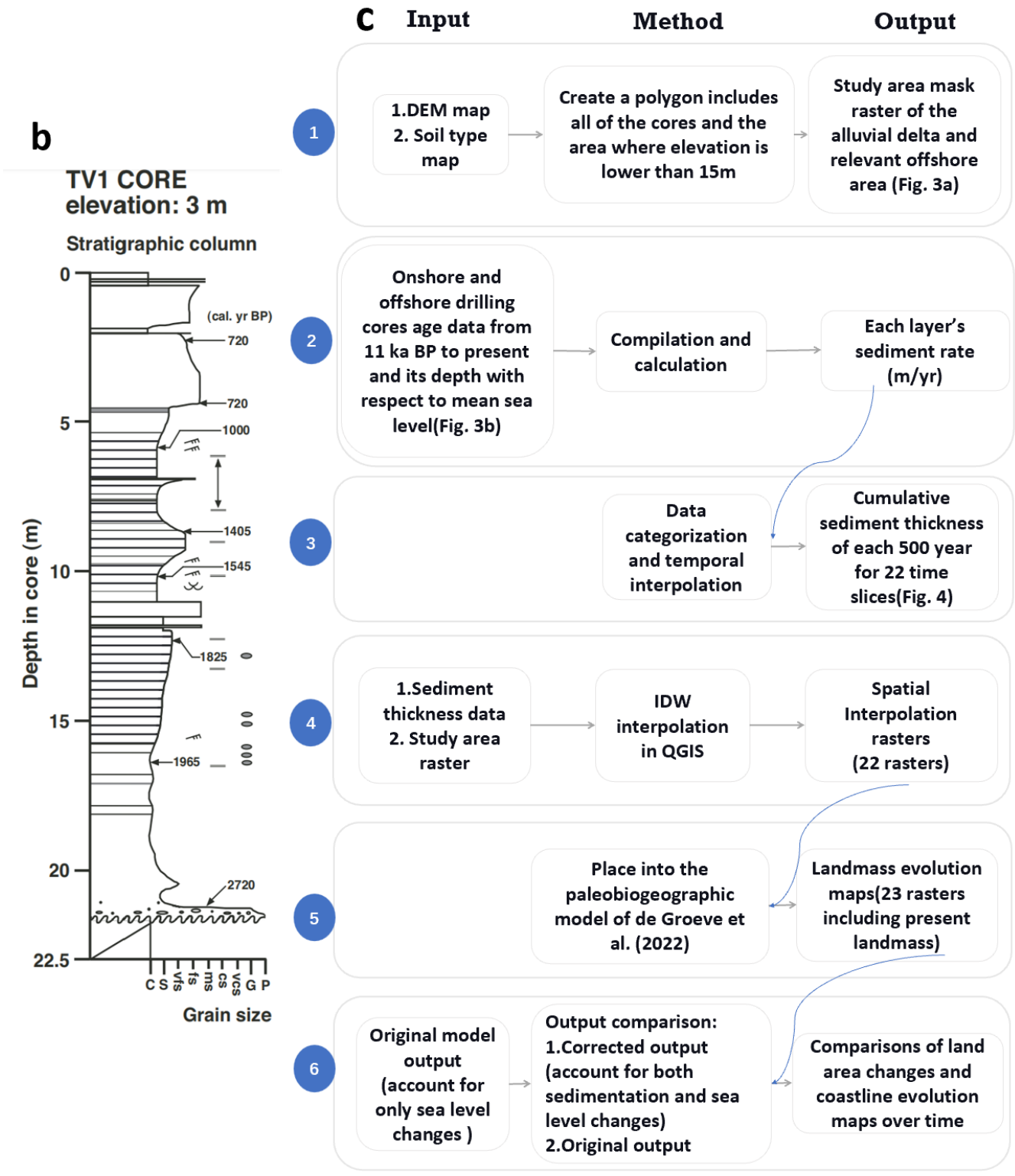

Fig.3. a. Study area and site of the cores which were included in this study. b. Example TV1 drilling core structure for data extraction (Source: Tanabe et al., 2003). c. General workflow for the reconstruction of the Mekong Delta Plain in this study (each step is illustrated in the following section).

The detailed methods are listed below, each step corresponds to Fig.3c:

2.1 Delta boundaries

It is necessary to focus on the area that is specifically affected by the delta alluvial sedimentary process, therefore taking geological or geomorphological settings into account to clip the study area (Fig.3a) which helps more precise interpolation further on would be needed. To do so, we created a new polygon that includes all of the cores and filter out the area by a masked raster with the rocky landscape by distinguishing terrestrial elevation higher than 15 m from the DEM map. For the marine portion, the boundary was drawn approximately along the shelf. In the meantime, using soil type maps in Vietnam and Cambodia as important references to interpret the result.

2.2 Data collection and compilation

Collect and extract onshore and offshore drilling core age data during the Holocene from previously published studies and the depths with respect to mean sea level are needed to model the paleo-coastline movement. All of the cores included in this study and their basic information are listed in Table 1 (onshore cores), Table 2 (offshore cores) and locations of the cores are presented in Fig.3a.

Data compilation begins with the calculation of sediment rate. Each core contains multiple sections with certain depths which represent stratigraphy and the history of deposition of a certain period (e.g. Fig.3b). Individual small section sediment rate calculation of the core requires four values: older strata depth in the entire core depth ($\boldsymbol{D_{start}}$) in meters as a starting depth and its corresponding estimated year ($\boldsymbol{Y_{start}}$) in year before present, and newer strata depth ($\boldsymbol{D_{\mathrm{end}}}$) as an ending depth with its corresponding year ($\boldsymbol{Y_{end}}$).

All of depths should be calibrated with the same reference with respect to the present-day mean sea-level ($\boldsymbol{MSL}$) by taking cores' elevations (in meters) into account. Define depths above sea level as positive value and below sea level as negative value (see Appendix I).

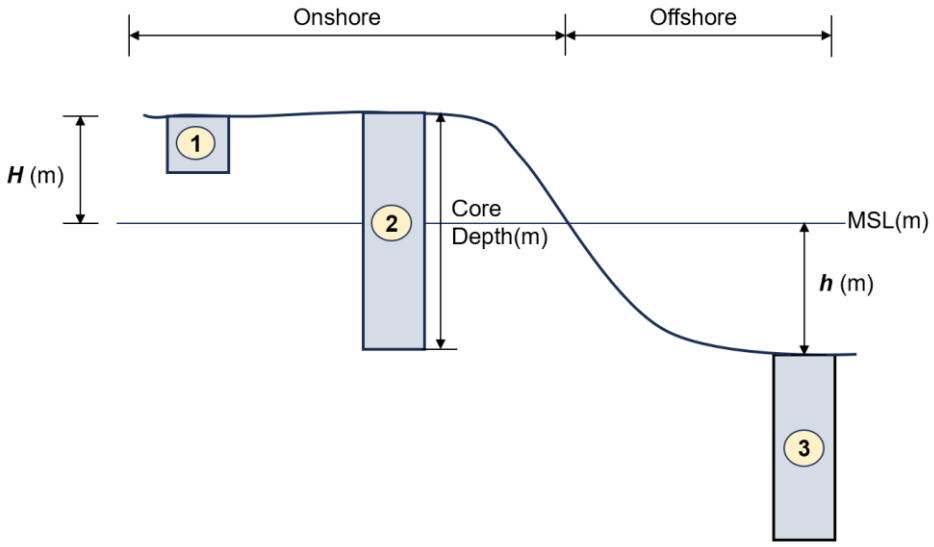

Fig.4. Three scenarios for core depth calibration (1 refers to onshore core case, total core depth does not exceed elevation height; 2 refers to onshore core case, total core depth exceeds elevation height; 3 refers to offshore core case).

There are three scenarios for depth calibration (as shown in Fig.4, listed by number 1,2,3). Here we use older strata starting depth as a calibration example ($\boldsymbol{D_{calibrated\_start}}$):

1) Onshore, total core depth does not exceed elevation height. Calibrated starting depth is connected with core's elevation with respect to MSL ($\boldsymbol{H}$) and its original depth (Eq.1).

$$D_{calibrated\_start\_1} = H - D_{start\_1} \quad (1)$$

2) Onshore, total core depth exceeds elevation height.

For the section does not exceed elevation height: calculation remains the same as scenario 1. For the section which exceeds elevation height, it can be calculated by Eq.2.

$$D_{calibrated\_start\_2} = H + D_{start\_2} \quad (2)$$

3) Offshore: As shown in Eq.3, calibrated depth is connected to water depth with respect to MSL ($\boldsymbol{h}$).

$$D_{calibrated\_start\_3} = h + D_{start\_3} \quad (3)$$

Calculations of all the ending depth ($\boldsymbol{D_{calibrated\_end}}$) in meters share the same principles as starting depth ($\boldsymbol{D_{calibrated\_start}}$).

The vertical accretion sedimentation rate ($\boldsymbol{S}$) of each core section in m/ky can be calculated by the following equation (Eq.3):

$$S = \frac{D_{calibrated\_start} - D_{calibrated\_end}}{Y_{start} - Y_{end}} \quad (4)$$

Table 1. Onshore core information which was included in this study.

Core name	Elevation /Water depth(m)	Latitude	Longitude	Materials	Time range (yrs BP)	Length of the core (m)	Reference
DT1	2	10°17′02″N	105°38′51″E	Plant material	11432-6881.5	25.5	Ta et al. 2005; Nguyen et al.2010
DT2	4	10°42'08"N	105°06'31"E	Plant material	7639-6572	9.44	Ta et al. 2020
DT3	7.5	10°41'20"N	105°24'03"E	Plant material	10077-4572	3.75	Ta et al. 2020
DT4	3.4	10°27'12"N	105°35'02"E	Plant material	4603-2239	18.03	Ta et al. 2020
3	2.5	10°47'39"N	105°21'03"E	Plant material	7466-4487	3	Ta et al. 2020
VL1	2	10°01′46″N	105°58′42″E	Plant material	6110-3435	34.11	Ta et al. 2002
TC1	2	9°41′04″N	106°26′48″E	Shell	5143-2883.5	14.92	Ta et al. 2002
TV1	3	9°51′04″N	106°11′37″E	Shell	2719.5-719	16.87	Ta et al. 2002
BT2	2	10°08′18″N	106°28′7″E	Shell/plant material	13304-3559.5	50.67	Ta et al. 2002
BT3	2	10°01′5″N	106°37′44″E	Shell/wood	4244-831.5	15.06	Ta et al. 2002
VLM	2	10°15'10"N	105°57'41"E	Organic matter	11313-4203	27.5	Ta et al. 2020
KS	7	11°28′49.74″N	105°07 ′12.42"E	Organic sediment/plant fragment	9140.5-664	24.05	Tamura et al. 2007
PK	6	11°11 ′32.82"N	105°16 ′38.28"E	Organic sediment/plant fragment	14239-1237.5	21.3	Tamura et al. 2009
PSG	3.5	10° 57' 33"N	105° 03' 37" E	Plant fragment	10348-1981	27.1	Tamura et al. 2009
CD1	1	9°32'51"N	106°15'16"E	Shell	3257-1476.5	11.17	Ta et al. 2005
GGM	2.3	10°45'6"N	105° 42' 40"E	Shell/plant remains	6485-1825	2.4	Proske et al. 2011
GGN	3	10°14'23"N	106°21'6"E	Wood	2025-0	1.49	Proske et al. 2011
TA	1.25	10°31'26"N	106°23'11"E	Carbonate shells	4630-0	3.5	Proske et al. 2010
GD	0.75	10°40.216′N	105°51.651′E	Plant remains	6890-5390	1.01	Proske et al. 2010
TD	0.75	10°39.731′N	106°12.928′E	Plant remains	6150-2870	0.45	Proske et al. 2010

MEK-1	18	12°15'30"N	105°33'14"E		280-90	3.25	Ishii et al.2020
MEK-2	15	11°55'45"N	105°12'13"E		470-190	3	Ishii et al.2020
MEK-3	16	11°54'48"N	105°12'05"E		470-220	1.35	Ishii et al.2020
MEK-4	14	11°52'43"N	105°09'03"E		490-440	1.1	Ishii et al.2020
MEK-5	8	11°11'49"N	105°15'59"E		540-190	1.85	Ishii et al.2020
MEK-6	6	11°11'37"N	105°16'19"E		110-60	1.25	Ishii et al.2020
MEK-7	5	11°11'28"N	105°16'50"E		130-60	0.7	Ishii et al.2020
MEK-8	12	11°46'32"N	105°01'25"E		5450-340	7.4	Ishii et al.2020
MEK-9	18	12°15'49"N	105°33'32"E		1160-840	4.975	Ishii et al.2020
MEK-10	15	11°57'22"N	105°11'31"E		4180-470	6.5	Ishii et al.2020
MEK-11	11	11°51'49"N	104°58'35"E		8940-1520	4.975	Ishii et al.2020
MEK-12	10	11°46'49"N	105°00'04"E		7370-2070	6.625	Ishii et al.2020
PA	8	11°43′50″N	104°57′51″E	Plant fragment/mug	8161.5-4434	3.7	Hori et al.2007
KL	7.6	10°22'45"N	104°26'44"E	Shell	3553-1742	1.15	Ta et al. 2020
ST3	2	9°29′ 57.84″N	106°1’49.08” E	Shell	7589-1486.5	19.46	Tamura et al. 2020
CM2	1	9°0’43.2” N	105°11’21.12” E	Shell/plant fragment	3349.5-180	18.46	Tamura et al. 2020
CM3	1	8°48’28.08” N	105°0’21.96” E	Plant fragment/shell	10211-80	27.24	Tamura et al. 2020
CM4	1	9°14’6” N	105°27’36” E	Shell/plant fragment	4731-735	14.89	Tamura et al. 2020
CM5	1.5	9°2’5.28” N	105°25’44.76” E	Shell/plant fragment	1157-510.5	7.73	Tamura et al. 2020
CM6	1.5	8°58’8.76” N	105°19’17.76” E	Shell/plant fragment	5763-394.5	19.12	Tamura et al. 2020

Note: 1) Elevations and water depths are all calibrated with respect to present-day mean sea-level.

2)Latitudes and longitudes are all set in DMS coordinate system.

3)All of the time ranges are from calibrated radiocarbon-14 dating data.

Table 2. Offshore core information which was included in this study.

Core name	Elevation /Water depth (m)	Latitude	Longitude	Materials	Time range (yrs BP)	Length of the core (m)	Reference
S62	56	9:15.00°N	107:59.18.6°E	Macro-fibers	13076-11670	7.9	Schimanski and Stattegger,2004
S65	48	9°23′15"N	107°45′2"E	Wood	10868-0	2.66	Schimanski and Stattegger,2004
S76	89	7°5′16 N	108°6′25 E	Shell/crustacean arm	9020-0	0.4	Schimanski and Stattegger,2004
S89	109	9° 16' 27" N	108° 39' 05.4" E	Wood, insoluble	14720-14120	0.87	Schimanski and Stattegger,2004
S91	115	9° 33' 54.6" N	108° 49' 36" E	Rotalia sp./sea urchin/pteropods/gastropod fragment	10956-5230	0.65	Schimanski and Stattegger,2004
S93	155	9° 45' 36.6" N	109° 07' 57" E	Shell	13670-750	19.655	Schimanski and Stattegger,2004
79-3	33	9°8’24” N	107°4’12” E	Peat	9421-0	2.39	Tjallingii et al.2014
81-2	28	9°15’28.8” N	107°19’58.8” E	Wood	10047-0	1.71	Tjallingii et al.2014
91-3	30	8°26’38.4” N	105°14’38.4” E	Plant material	10047-0	3.1	Tjallingii et al.2014
93-2	31	8°23’16.8” N	105°6’46.8” E	Wood	9667-0	3.64	Tjallingii et al.2014

96-3	28	8°24’28.8” N	104°34’15.6” E	Bivalve	8858-0	2.08	Tjallingii et al.2014
100-3	32.5	8°31’26.4” N	104°20’9.6” E	Bivalve	9306-0	2.78	Tjallingii et al.2014
115-2	32	8°7’1.2” N	105°36’10.8” E	Wood	9210-0	2.82	Tjallingii et al.2014
70-2	43	10°22’15.6” N	108°0’43.2” E	Plant material	10862-0	3.1	Tjallingii et al. 2010
73-3	31	10°14’9.6” N	107°16’44.4” E	Wood	9037-0	3.55	Tjallingii et al. 2010
69-2	42	10°23’2.4” N	108°0’46.8” E	Gastropod/Echinoderm	8855-8635	0.65	Tjallingii et al. 2010
106-2	26	8°11’13.2” N	104°33’43.2” E	Wood	10054-0	5.1	Tjallingii et al.2014
109-2	32	8°6’57.6” N	105°14’31.2” E	Wood	10435-0	3.84	Tjallingii et al.2014
114-3	32	8°6’57.6” N	105°35’31.2” E	Wood	10645-0	4.72	Tjallingii et al.2014
68-3	60	10°16’51.6” N	108°25’19.2” E	Wood, shell, plant material	11984-180	4.2	Tjallingii et al. 2010; Tamura et al. 2020
CJB01-64	62	6°0’0” N	104°58’12” E	Plant debris/shell/Mixed benthic foraminifera	12252-3296	0.43	Wu et al.2023
CJB01-75	80	4°54’36” N	105°31’48” E	Mixed benthic foraminifera	3715-1473	0.13	Wu et al.2023
BT-7	47	9°6’36” N	100°55’12” E		13300-1465	0.12	Wu et al.2023
MD05-2893	4.5	6° 6’4.32” N	110°40’43.43” E	Mixed foraminifers/G.ruber	15667-1557	1.47	Jiwarungrueangkul et al.2019
MKII03	15.6	9° 50’27.6” N	104°24’28.8” E		1570-50	0.25	Xue et al.2009
MKII07	10	9°7’30” N	104°44’34.8” E		3120-800	0.16	Xue et al.2009
MKII09	10	8°48’3.6” N	104°33’39.6” E		845-830	0.6	Xue et al.2009
MKII14	16	8°30’43.2” N	105°17’16.8” E		1800-1350	0.3	Xue et al.2009

Note: 1) Elevations and water depths are all calibrated with respect to present-day mean sea-level.

2)Latitudes and longitudes are all set in DMS coordinate system.

3)All of the time ranges are from calibrated radiocarbon-14 dating data.

2.3 Temporal interpolation

Following data retrieval, we next performed linear interpolation and integrated the sedimentation rates S (m/yr) into regular 500-year intervals, between 11 ka BP and the present (In total 22 time slices). The output will be cumulative sediment deposition thickness within the 500-year bracket.

2.4 Spatial interpolation

We use the Inverse Distance Weighting Interpolation function (IDW) to determine sedimentation rates across the study area. The basic distance weighting function definition is given by Eq. (5), (Shepard,1968).

$$v_{(x)} = \frac{\sum_{i=1}^{N} w_i \cdot v_i}{\sum_{i=1}^{N} w_i} \quad (5)$$

Here, $\boldsymbol{x}$ and $\boldsymbol{v_{(x)}}$ is a point in the study area and its estimated value, $\boldsymbol{N}$ is the total number of known points used in interpolation. $\boldsymbol{v_i}$ is the known value at each of the $\boldsymbol{i}$ point and $\boldsymbol{w_i}$ is the weights, calculated based on $\boldsymbol{d}$ and $\boldsymbol{p}$.

For areas without measured rates, this method assigned deposition rates based on published deposition rate measurements from nearby areas.

$$w_i = \frac{1}{d(x, x_i)^p} \quad (6)$$

Besides, the outcome would be highly dependent on the weighting coefficient setting. Eq. (6) follows the definition of weighting based on distance coefficient. Where $\boldsymbol{d}$ is the distance between known points and unknown points $\boldsymbol{x}$. $\boldsymbol{p}$ is the power distance weighting coefficient. Weighting controls the rate how the weighting influence will decrease as the distance from the new point increases. The bigger the distance weighting coefficient, the interpolated unknown values are more likely to be influenced by the closest data points. However, it might lead to a less smooth surface. (Spatial Analysis - Interpolation, 2024)

Overall, the weighting coefficient was set as 2 for the best program performance, since after experimentally setting it lower would change the original data value in the raster and affect output accuracy. Assigning artificial values on the boundary of the study area polygons as 0 to assure the precision of the interpolations. 22 rasters of each interval would be generated by resampling the rates onto a study area local grid with 811 rows and 1089 columns suitable for input to the numerical paleo-coastline model.

2.5 Landmass result acquisition

We used the tabs (Temporal Altitudinal Biogeographical Shifts) R-package to reconstruct the paleo-coastline of the Mekong Delta (https://gitlab.com/uva_ibed_piac/tabs). Tabs allows to reconstruct coastlines accounting (1) both for spatial variations in sea-level positions using the spatial explicit sea-level model published by De Groeve et al. (2022) and further local corrections, for instance due to geotectonic uplift and subsidence, or delta sedimentation and erosion. In this study we reconstructed the coastline by combining spatial-explicit sea-level model, with the cumulatively summed sedimentation rasters. We also generated a paleo-coastline original reconstruction which only accounts for sea-level changes to compare the difference in area change and coastline shifts over time.

2.6 Reconstruction comparison

Comparing and the original model output from model of De Groeve et al. (2022) with corrected grids (where the correction grids express the cumulative sedimentation) can see the difference of the coastline movements account for both sedimentation and sea-level changes and account for only sea-level changes. The objective of the comparison is to see the difference of land area changes over time in both cases and coastline evolution difference in patterns over time.

To obtain reconstructions from De Groeve et al. (2022), extracting coastline vectors and landmass polygons from landmass output raster to calculate area in square kilometer in QGIS were required.

3.Results

3.1 Spatial pattern shown by interpolations

The spatial patterns of sediment deposition are strongly influenced by the direction of water flow and elevation. It follows a certain consecutive trend, while certain regions have higher sediment accumulation compared to the others. The interpolation rasters in Fig.5 are based on cumulative sediment thickness per 500 years of each time slice, with adding the values up each time step. For instance, to get the 3 ka BP accumulated sediment raster, summing the accumulated thicknesses of consecutive rasters from 500 BP up to 3000 BP is required.

For the onshore part, the areas near the eastern coastline constantly show a higher cumulative sedimentation trend throughout the whole Holocene than the western counterpart. A few eastern coastal locations retain relatively high sediment thickness over time.

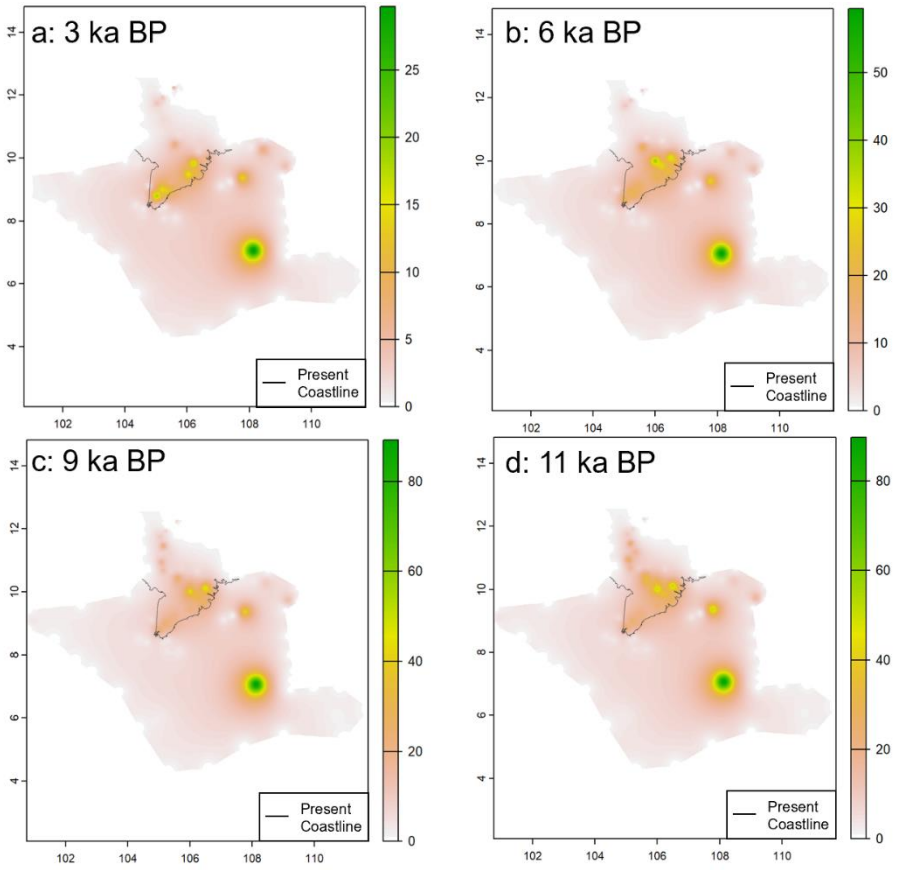

Fig.5. Input sediment accumulative thickness interpolation rasters operated by Inverse Distance Weighting (IDW) for different time before putting it into the palae-coastline model. [Note:1) These rasters do not represent temporal trend of sediment accumulation but only spatial patterns; 2) Color scale ranges in different plots are different]

3.2 Temporal patterns of significant deposition cores

Cores positioned in various locations exhibit instinctive patterns over time, with cores that are close to each other showing a similar trend of periods with high sediment deposition. Temporal patterns of sediment deposition thickness of six example cores are presented in Fig.6.

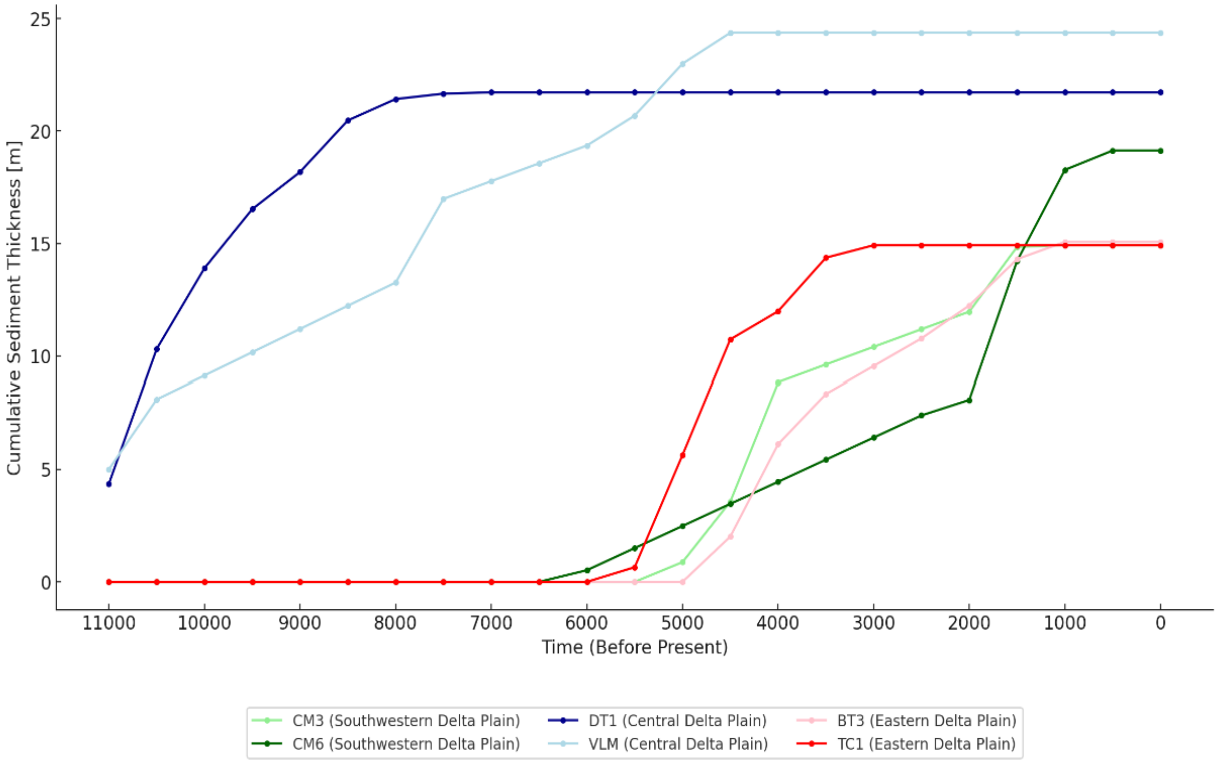

Fig.6. Cumulative sediment thickness for example cores in different locations.

As shown in Fig.3a, core CM3 and CM6 are located on the southwestern delta plain. Sediment was deposited mainly at the recent phase, spanning from 3.5 ka to 0.5 ka, with a particularly significant deposition trend from 1.5 ka to 1 ka.

TC1 and BT3 share similar patterns of sediment thickness over time as both of them are located at the eastern delta plain. The sedimentation processes were active specifically during the Late Holocene from 4.5 ka to 3 ka.

Core VLM and DT1 are located at the central delta plain, as shown in Fig.6, significant deposition happened around the Early Holocene period from 11 ka to 7.5 ka, indicating that this area might have undergone formation earlier than other areas.

However, we also need to consider that not all of the historical data of the cores were recorded up to 11 ka BP, so it might cause some comprehension differentiation on the temporal pattern of the sediment deposition. Not all the cores in the near neighbor share the same pattern as the example cores, indicating the occurrence of temporal variation.

3.3 Coastlines and delta landmass evolution during the Holocene under the influence of sea-level changes

The key point to investigate the complex landmass and coastline dynamics of the VMD is to look into the sea-level curve effect combined with its collateral impact on seafloors based on the sediment deposition input. The landmass changes of the VMD can be divided into three phases (Fig.7), corresponding to three sea-level change phases: Initial Transgression[4] Phase (corresponds to Phase C in Fig.1), Intermediate Phase (corresponds to Phase B in Fig.1), and Later Progradation[5] Phase (corresponds to Phase A in Fig.1).

Initial Transgression Phase (11-7 ka BP): During this phase, the global sea and land structure has gone through rapid changes because of rapid sea-level rise. The Mekong Delta area experienced transgression, there was a noticeable decrease in landmass according to Fig.7c. In the meantime, shelf area expansion and coastline retreat were noticeable (Fig.8c). Most of the delta area was submerged underwater at the end of this phase.

Intermediate Phase (7-4 ka BP): The shrinkage of land slowed down and stayed relatively stable (Fig.7a&b). It corresponds to the high stand of sea level followed by the deceleration of sea-level rise after initial transgression phase.

Later Progradation Phase:(4 ka BP - present): During this period, Fig.7a&b shows the Mekong Delta was initiated and became a regressive[6] delta because of sea level lowering from the high stand alongside with high deposition rate (Tamura et al., 2012). A large accumulation of clayey sediments has been trapped in the subaqueous area causing rapid progradation rate around 50 m/yr (Xue et al., 2009; Zoccarato et al., 2018). The coastline moved initially towards the south of the original land and then towards the southwestern part of the sea (Fig.8a&b). For the last 6 ka, the delta has progradated more than 200 km around the Cambodian border to the present coastline in southern Vietnam (Ta et al., 2002; Liu et al., 2017)

[4] Transgression: Coastline landward migration because of relative sea-level rise or low sediment supply (Nienhuis et al., 2022).

[5] Progradation: Coastline seaward migration because of rapid relative sea level fall or high sediment supply. (Nienhuis et al., 2022)

[6] Regression: The same definition as progradation.

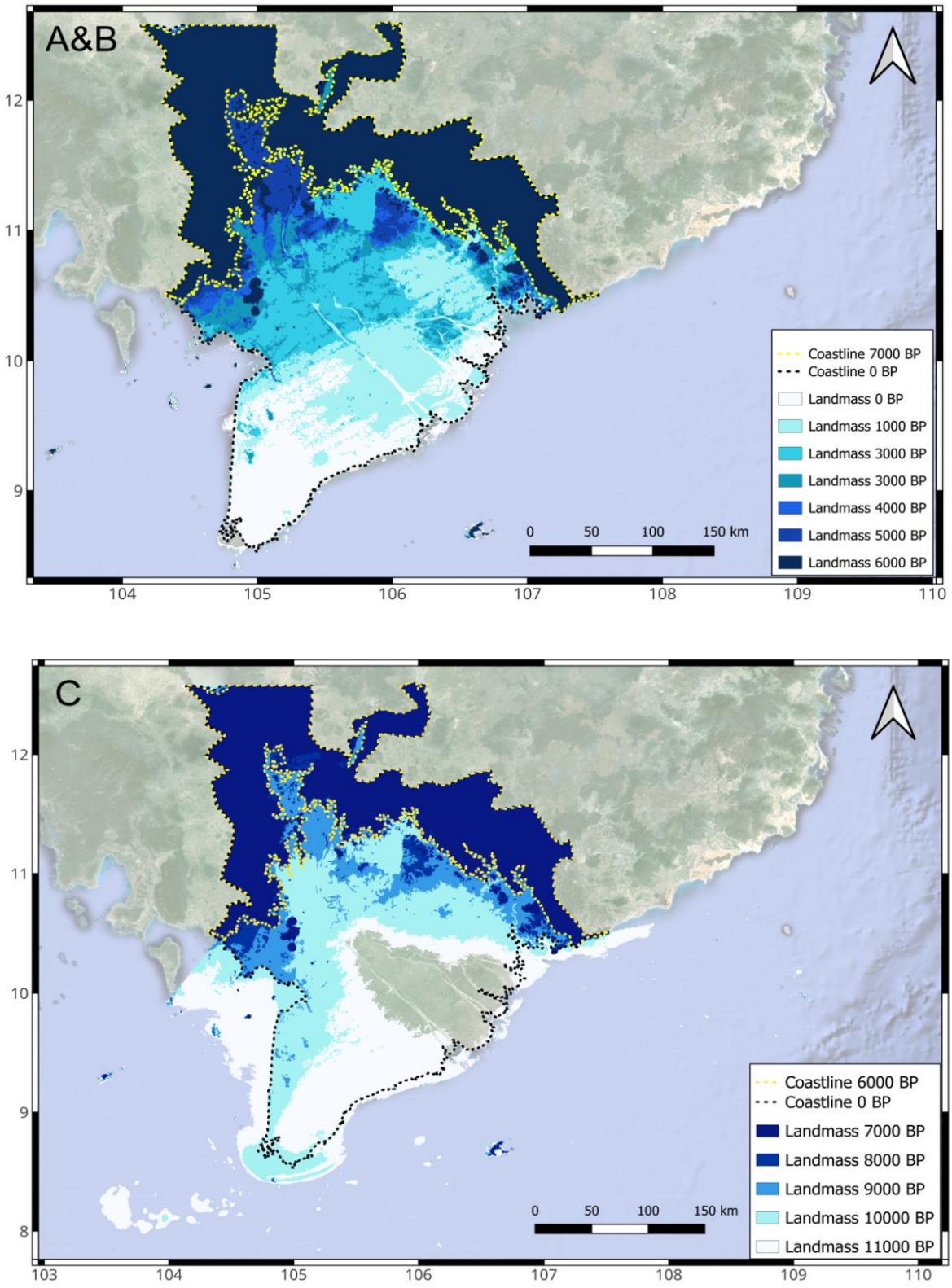

Fig.7. **a&b.** Land evolution maps from 6 ka BP to present (corresponds to sea level in Phase A&B in Fig.1).

c. Land evolution maps from 11 ka BP to 6 ka BP (corresponds to sea level in Phase C in Fig.1).

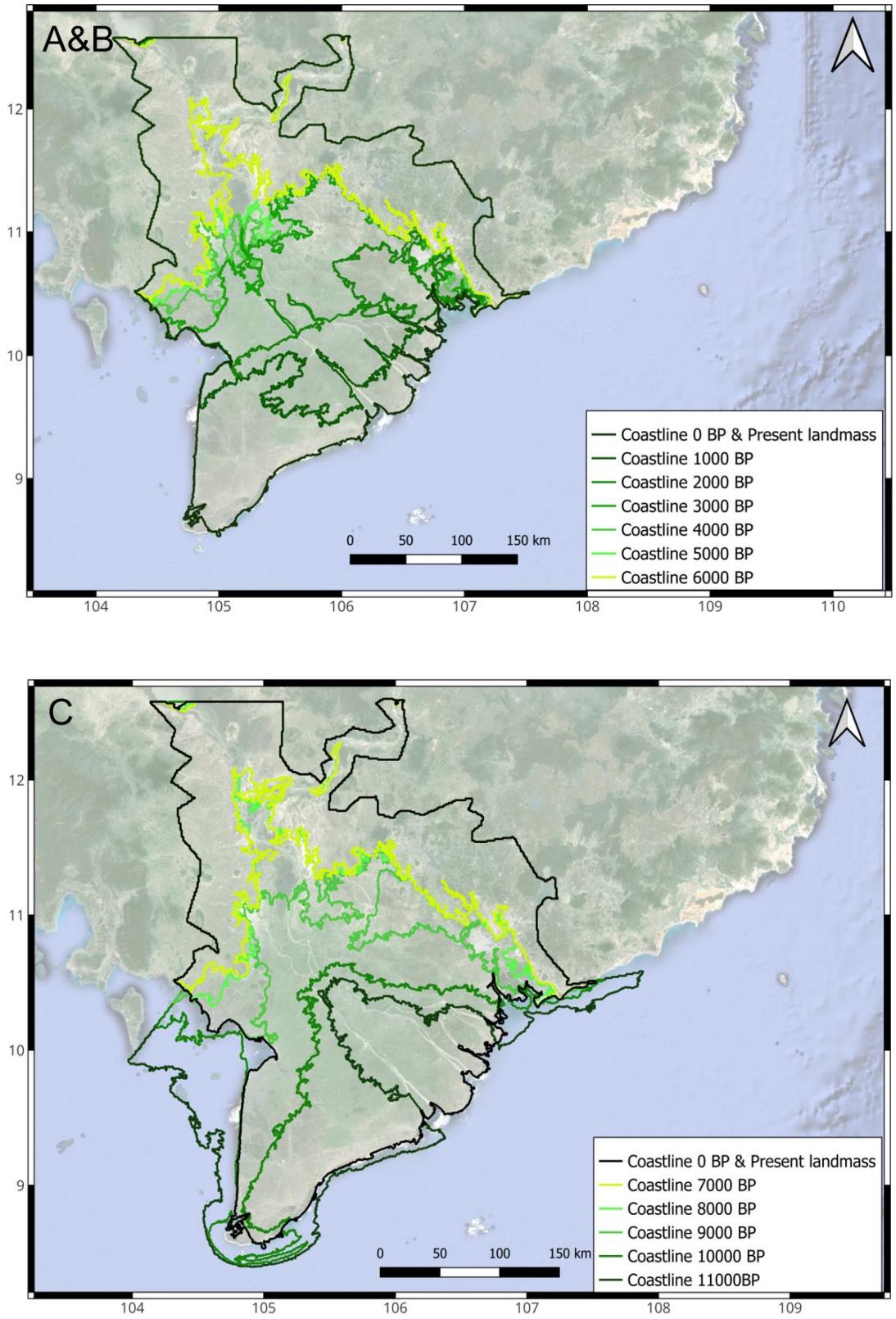

Fig.8. **a&b.** Coastline evolution maps from 6 ka BP to present (correspond to sea level in Phase A&B in Fig.1). **c.** Coastline evolution maps from 11 ka BP to 7 ka BP (correspond to sea level in Phase C in Fig.1).

3.4 Model output comparison

When comparing the original model (sorely accounts for sea-level change) from De Groeve et al. (2022) with the corrected model (includes sedimentation together with sea-level change), differences in coastline movements and land area changes become apparent.

To better understand the differences in findings, Fig.9 presents a schematic framework comparing the present coastline and coastline at 11 kyr BP. The effect of sedimentation makes land area increase less at 11000 BP compared to if we assume that there was no sedimentation. Details of the landmass area change statistics are listed in Table 3.

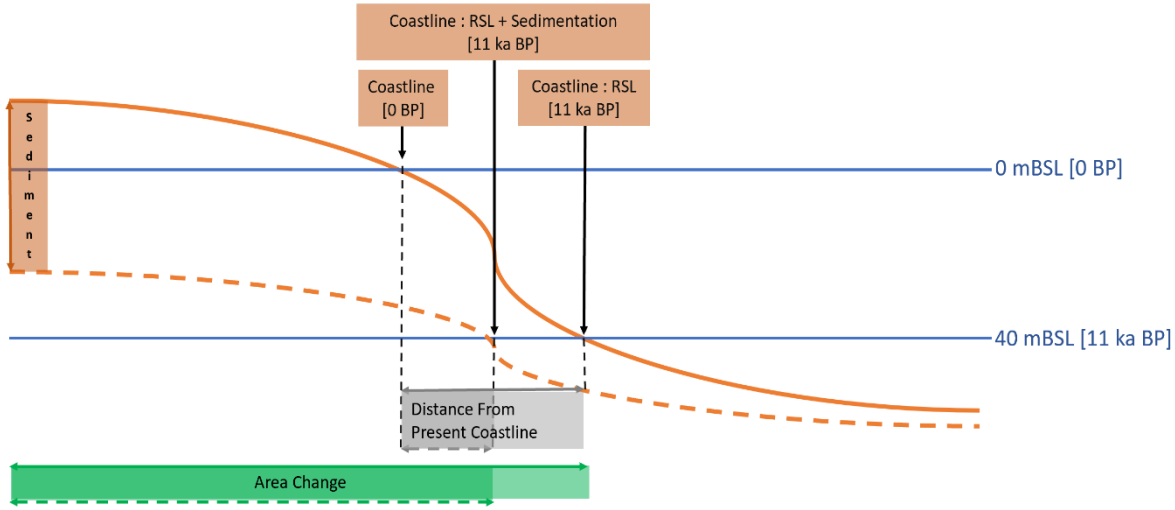

Fig.9. Schematic figure for understanding coastline reconstructions of 0 and 11 ka BP.

Table 3. Area change from 11 ka BP to the present of corrected and original model output.

Model output	Area (km^2)	Area change from 11 ka BP to the present (km^2)
Present landmass	83508.934	-
Corrected model landmass for 11 ka BP	88041.585	4,532.651
Original model landmass for 11 ka BP	118144.864	34,635.93

However, this trend does not only happen to the coastline in this year, past coastlines were generally more land inwards when we account for the sedimentation under the same sea-level change conditions. Fig.10 shows coastline evolution from 11 ka BP to the present, with taking certain years as examples.

By comparing the main landmass area, we can see how much difference the two models' outputs produce. The corrected coastline model output at 6 and 7 ka BP in this study aligns relatively closely with the original output, as evidenced that over 80% of the landmass overlaps in the results from the two models, as indicated in Table 4. Coastlines at 2 and 11 ka BP of the two models results show slightly more distance than the former two cases, with overlapping land percentages ranging from 69- 75%. The most notable discrepancy in coastline positionings occurs at 4 ka BP, with only 50% of land overlapped in the two models.

In all cases, considering sedimentation into the model tends to moderate variations in coastline changes based on sea-level changes. Besides, the eastern coastlines experienced a lesser degree of coastal retreat, while western coastlines shifted inland more dramatically and presented a less smooth appearance.

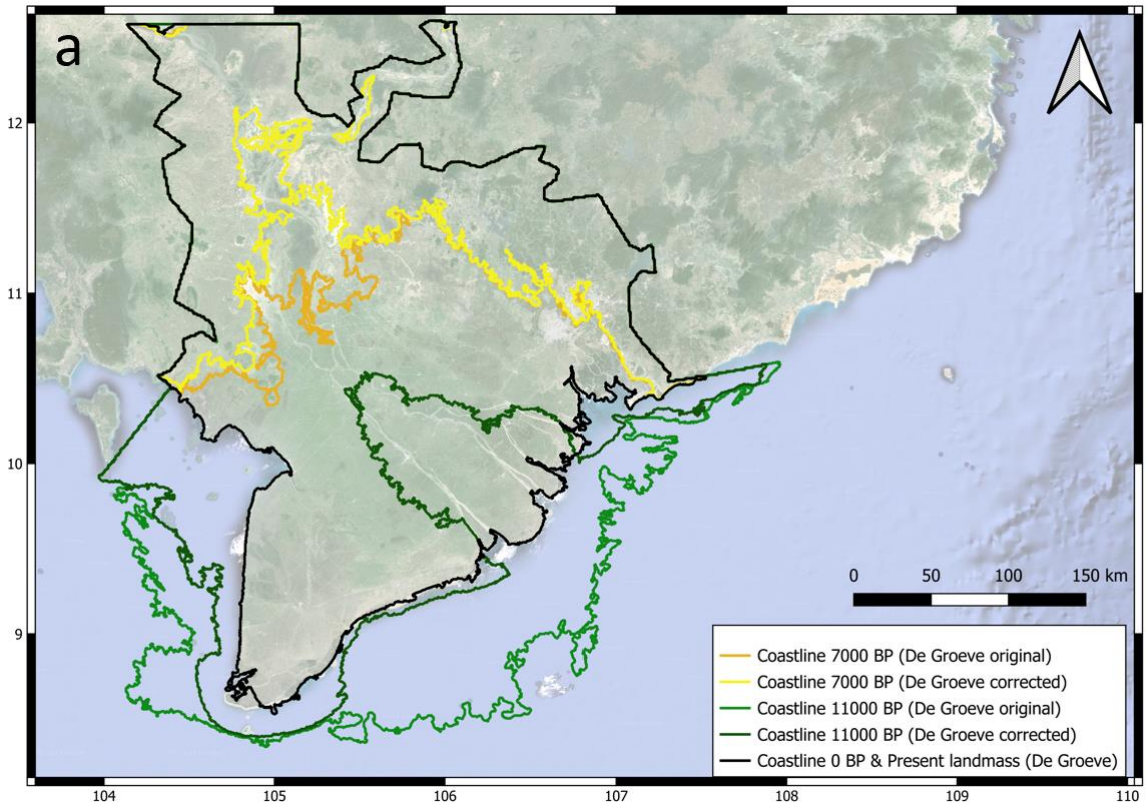

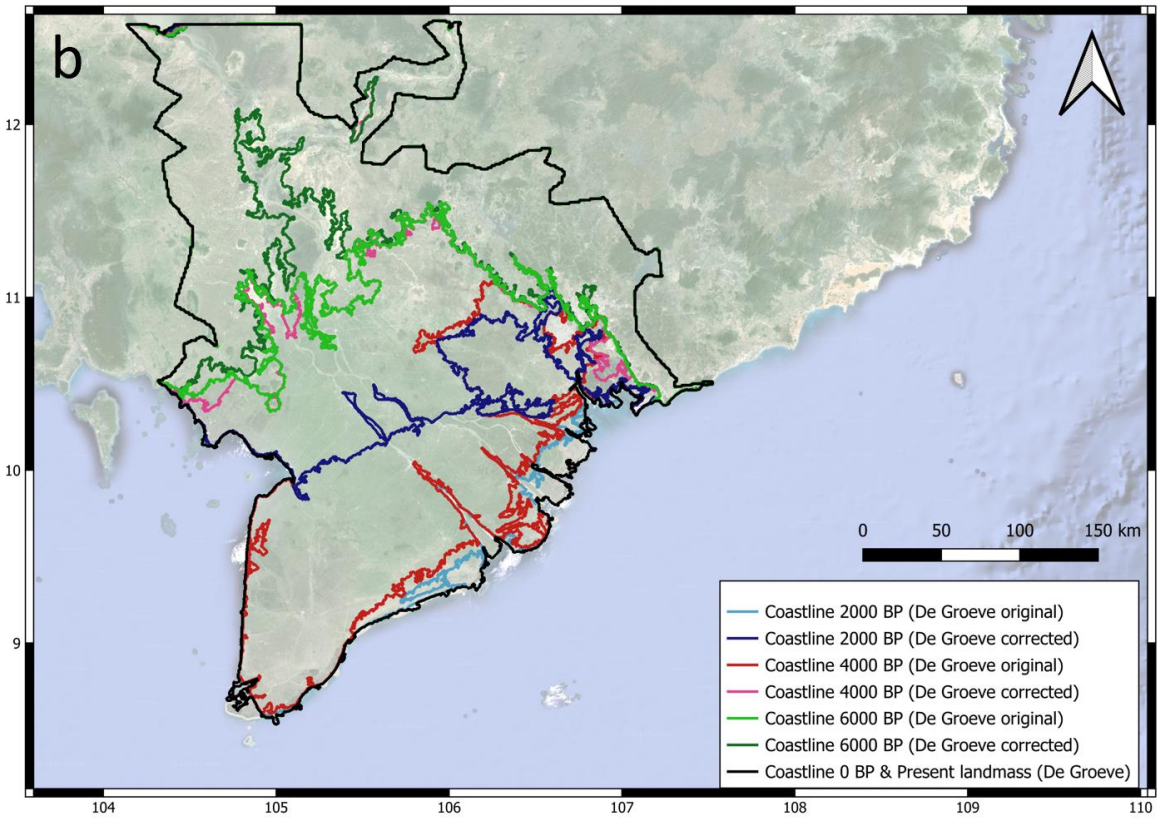

Fig.10 a. Reconstructed coastline position of original model and corrected model (De Groeve et al. 2022) at 7 ka BP and 11 ka BP. b. Reconstructed coastline position of original model and corrected model (De Groeve et al. 2022) at 2 ka BP ,4 ka BP and 6 ka BP.

Table 4. Overlapping area of corrected and original model output in different year.

Time	Area for corrected model (km2)	Area for original model (km2)	Overlap area
11 ka BP	88041.585	118144.864	74.52%
7 ka BP	29457.979	36316.110	81.11%
6 ka BP	30534.117	36316.528	84.07%
4 ka BP	37217.144	73602.527	50.56%
2 ka BP	55970.748	80934.989	69.15%

Note: The areas only include the main landmass, which means segmentation lands and islands are not included.

4.Discussion

4.1 Application on species evolution

Integrating sediment dynamics into paleo-coastline models offers a more comprehensive framework for understanding the relationships between geomorphology and biological aspects in the Mekong Delta. The spatial and temporal shifts in the coastline and the connectivity of marine passages play crucial roles in shaping the biodiversity, species distribution, migration, and evolutionary trends of both marine and terrestrial biota. They vary in intensity, scale, duration, and direction, adding complexity to the entire biogeographical system (Hanebuth et al., 2010).

According to the result, after the inundation of the low gradient delta from 11 ka BP to 7 ka BP, the pushback of the shoreline (Fig.8c) reduced land area and eliminated land connections and freshwater river connections within the delta. Onshore populations that were once connected became isolated from each other. Besides, it would cause constant coastal flooding invasion to salt-sensitive forests and grassland vegetation near the coast. (Sathiamurthy and Voris, 2006; Hanebuth et al., 2010; Salles et al., 2021). This inundation adversely created an opening of the ocean passages which led to an expansion and stronger connection of aquatic habitats between the South China Sea and the Gulf of Thailand, enabling marine species to move into central delta plains that were previously landlocked by land barriers. It also facilitates both the arrival of new marine species, such as mangroves on tidal flats and the expansion of existing populations (Hanebuth et al., 2010).

Time range during the intermediate phase from 7 – 4 ka BP with relative static landmass change offers terrestrial vegetation recovery time to form mature biota communities (Hanebuth et al., 2010).

Nevertheless, since delta progradation happened from 4 ka BP (Fig.7a&b), the dispersal of land-based species was promoted due to the extension of the land area. In the meantime, this change also hindered the marine connectivity between the South China Sea and the Gulf of Thailand that had been established earlier. Intertidal marine communities, such as mangroves were being pushed seaward, leading to the creation of a complex and unstable zone of ecological succession (Hanebuth et al., 2010).

Inhabited humans' migration also would be affected by the continent shelf movement. The changes in gateways prompted population differentiation in the VMD from the signs of migration rate, population size, and split (Kim et al.,2023).

This investigation enhances the accuracy of predictions of potential future changes in biodiversity in response to deltaic environmental changes by investigating the long-term effects of sediment dynamics on ecosystem functioning in the past. It could also provide insight into how to give timely responses to changes to safeguard sustainable ecosystem services for the future.

4.2 Input dataset features

4.2.1 Ice-loading (isostasy adjustment), sediment mass redistribution and sea-level rise are included in the model

The primary vertical movements in the Mekong Delta region during the Holocene would have been subtle and influenced mainly by isostatic adjustment and sediment mass redistribution.

In this study, the palae-coastline model of De Groeve et al. (2022) has been used for a better understanding of the biogeographical and archaeological aspects of the VMD. The model not only includes sea-level variation as the basic factor affecting coastline movement but also adjusts seafloors dynamically to geophysical changes (spatial-explicit sea-level model).

To reconstruct coastlines more accurately, it is essential to apply glacial-isostatic models that incorporate the depression of the Earth's crust under seawater loading. The model also considers the spatio-temporal distribution of paleo-ice sheets and their impacts on the Earth's crust and its pulling-up effect on seawater. Additionally, the redistribution of seawater on the planet is considered in this model as well.

The method increases the accuracy of the reconstructions and coastline retreat rates and shelf expansion rates would be closer to the reality.

4.3 Improvement

4.3.1 Does not include tectonic uplift

The Mekong River Delta is situated on the southeastern margin of the Eurasian Plate. Over the past 11,000 years, the tectonic activity in the Mekong Delta region has been relatively stable, compared to the other active tectonic regions along plate junctions (Hanebuth et al., 2010; Liu et al., 2017). Consequently, this study explicitly excludes considerations of tectonic uplift from its analysis.

However, a significant amount of the sediment is originally from the Tibetan Plateau, which is located in the upper Mekong. This area features active tectonic activities, alongside intense summer monsoon. Therefore, the dynamic tectonic strain and the precipitation-driven river incision continue to be important sources of sediment input for the Mekong Delta (Gupta,2009). Overlooking these factors would affect the precision of the result because the net sediment input might be underestimated.

4.3.2 Does not include erosion rate

The interplay of sediment deposition and erosion in channels plays an important role in controlling the geomorphologic development of the delta area (Hung et al., 2013).

While deposition is fundamental to the aggradation and spatial expansion of deltas, the function of erosion is to reshape it by removing sediments from one location and then transporting them to another location where they would be deposited (Liu et al., 2017). Erosion does not only exist in channels but also floodplains or deltic coastal regions. Coastal erosion is primarily driven by rising sea levels, with extensive and rapid features affecting coastline movements (Erban et al., 2014). This dynamic shows the complexity and instability of deltaic landscapes, posing challenges to monitor and track down deltaic movement in a scientific way. Besides, riverbank erosion is a natural process but can be strongly accelerated by human activities. It highlights the intricate connection between natural dynamics and anthropogenic interventions within deltaic systems.

In this study, the scope has been specifically narrowed to examine only the role of sediment deposition in the geomorphological evolution of the VMD. It would generate a more dynamic fluctuating growth and loss of the areas on the coast if erosion had been integrated for a comprehensive investigation.

4.3.3 Does not contain enough sediment core data from the western part of the delta

In this analysis, the majority of the accessible core data is located in the eastern sector of the delta. It can be observed that the consistency of the eastern coastline is superior to that of the western part. The regional variability of the western sector has been underestimated. It indicates the need for further data acquisition to enable comprehensive analyses in the western area.

4.3.4 Does not include subsidence rate

The combination of natural and anthropogenic factors significantly influences its subsidence rate within the delta.

The VMD is characterized by its formation from mainly unconsolidated, fine-grained (clayey) sediments, that make the delta plain vulnerable alongside its low elevation to sea-level rise. The changing natural compaction rates could easily alter sedimentation in this region. This vulnerability is further compounded by human activities such as groundwater pumping, infrastructural loading, sand mining, and dam construction (Zoccarato et al., 2018). Since the 1980s, the region has confronted the integrated challenges of land subsidence, with rates reaching up to 20 mm per year, and the accelerating rise in sea level, making it urgent for the VMD to implement a better strategy to tackle increasing inundation risks, salinity intrusion and erosion, which might threaten agriculture, infrastructure, and livelihoods of the delta's inhabitants (Erban et al., 2014; Liu et al., 2017).

The scale of shoreline erosion and land loss in this study has been underestimated without taking subsidence into account. In addition, river channels and the banks of the delta might have also been eroded strongly by coastal floodings because of land elevation loss (Liu et al., 2017).

Assessing subsidence rates requires an estimation of soil porosity. The challenge is reconstructing historical environmental conditions over such a prolonged period requires a relatively consistent historical dataset, but the scarcity of comprehensive data represents a limitation in the understanding of the subsidence rate before the Industrial Revolution Period.

5.Conclusion

This study solves the knowledge gap and generates a more precise reconstruction of the Mekong-Sunda Shelf region where sedimentation plays an important role in morphological changes, based on the methods including sedimentation, sea-level changes and their side effects.

Putting sedimentation effect into the paleo-coastline model has strengthened the understanding of the Holocene evolution and its implication for species evolution of the Mekong River Delta. The result has shown the interplay of sea-level rise and sedimentation generated three distinct phases of the delta's landmass evolution and form today's landscape. The delta's initial transgression trend was followed by a delta progradation caused by sea level falling aligned with significant sediment deposition. The landmass dynamics of the Mekong Delta have influenced the timing of the exposure and disappearance of the gateway between other Sunda shelf components. Looking into the result is beneficial to have a better understanding of the biodiversity and species evolution in this area.

By bridging knowledge gaps with innovative modeling approaches and comprehensive data analysis, this study could provide a robust framework for past and future insight into paleobiogeography on a global scale.

Reference

Albers, E. (2023). Solving Deltas with Deltas: Simulating fluvial deltaic progradation to reconstruct paleo coastline responses to sea-level rise in the Gulf of Amfrakikos in Greece since the Holocene. Bachelor Thesis. University of Amsterdam.

Gupta, A. (2009). Geology and landforms of the Mekong Basin. Centre for Remote Imaging, Sensing and Processing. The Mekong. Chapter 3.

De Groeve, J., Kusumoto, B., Koene, E., Kissling, W. D., Seijmonsbergen, A. C., Hoeksema, B. W., Yasuhara, M., Norder, S. J., Cahyarini, S. Y., van der Geer, A., Meijer, H. J. M., Kubota, Y., & Rijsdijk, K. F. (2022). Global raster dataset on historical coastline positions and shelf sea extents since the Last Glacial Maximum. Global Ecology and Biogeography. 31, 2162-2171.

Dunn, F. E., & Minderhoud, P. S. J. (2022). Sedimentation strategies provide effective but limited mitigation of relative sea-level rise in the Mekong delta. Communications Earth & Environment, 3(2). https://doi.org/10.1038/s43247-021-00331-3

Erban, L. E., Gorelick, S. M., & Zebker, H. A. (2014). Groundwater extraction, land subsidence, and sea-level rise in the Mekong Delta, Vietnam. Environmental Research Letters, 9(8), 084010. https://doi.org/10.1088/1748-9326/9/8/08401

Ferrier, K. L., Mitrovica, J. X., Giosan, L., & Clift, P. D. (2015). Sea-level responses to erosion and deposition of sediment in the Indus River basin and the Arabian Sea. Earth and Planetary Science Letters. http://dx.doi.org/10.1016/j.epsl.2015.01.026

Hanebuth, T. J. J., Voris, H. K., Yokoyama, Y., Saito, Y., & Okuno, J. (2010). Formation and fate of sedimentary depocentres on Southeast Asia's Sunda Shelf over the past sea-level cycle and biogeographic implications. Earth Science Review.
https://doi.org/10.1016/j.earscirev.2010.09.006

Hung, N. N., Delgado, J. M., Güntner, A., Merz, B., Bárdossy, A., & Apel, H. (2014). Sedimentation in the floodplains of the Mekong Delta, Vietnam Part II: Deposition and erosion. Hydrological Processes, 28(13), 3145–3160. https://doi.org/10.1002/hyp.9855

Ishii, Y., Tamura, T., & Ben, B. (2021). Holocene sedimentary evolution of the Mekong River floodplain, Cambodia. Quaternary Science Reviews.
https://doi.org/10.1016/j.quascirev.2020.106767

Jiwarungrueangkul, T., Liu, Z., & Zhao, Y. (2019). Terrigenous sediment input responding to sea-level change and East Asian monsoon evolution since the last deglaciation in the southern South China Sea. Global and Planetary Change, 174, 127–137.
https://doi.org/10.1016/j.gloplacha.2019.01.011

Kim, H. L., Li, T., Kalsi, N., Nguyen, H. T. T., Shaw, T. A., Ang, K. C., Cheng, K. C., Ratan, A., Peltier, W. R., Samanta, D., Pratapneni, M., Schuster, S. C., & Horton, B. P. (2023). Prehistoric human migration between Sunda land and South Asia was driven by sea-level rise. Communications Biology, 6(150). https://doi.org/10.1038/s42003-023-04510-0

Li, X., Liu, J. P., Saito, Y., Nguyen, V. L. (2018). Recent evolution of the Mekong Delta and the impacts of dams. Earth-Science Reviews, 181, 28-46. https://doi.org/10.1016/j.earscirev.2018.04.008

Li, Z., Saito, Y., Mao, L., Tamura, T., Li, Z., Song, B., Zhang, Y., Lu, A., Sieng, S., & Li, J. (2012). Mid-Holocene mangrove succession and its response to sea-level change in the upper Mekong River delta, Cambodia. Quaternary Research. 10.1016/j.yqres.2012.07.001

Liu, J. P., DeMaster, D. J., Nguyen, T. T., Saito, Y., Nguyen, V. L., Ta, T. K. O., & Li, X. (2017). Stratigraphic formation of the Mekong River Delta and its recent shoreline changes. Oceanography, 30(3), 72-83. https://www.jstor.org/stable/10.2307/26201900.

Manh, N. V., Dung, N. V., Hung, N. N., Merz, B., & Apel, H. (2014). Large-scale suspended sediment transport and sediment deposition in the Mekong Delta. Hydrology and Earth System Sciences. 10.5194/hess-18-3033-2014

Milliman, J. D., & Syvitski, J. P. M. (1992). Geomorphic/ tectonic control of sediment discharge to the ocean; the importance of small mountainous rivers. The Journal of Geology. 100, 525-544.

Minderhoud, P. S. J., Coumou, L., Erkens, G., Middelkoop, H., & Stouthamer, E. (2019). Mekong delta much lower than previously assumed in sea-level rise impact assessments. Nature Communications, 10(3847). https://doi.org/10.1038/s41467-019-11602-1

Nguyen, V. L., Ta, T. K. O., & Tateishi, M. (1998). Late Holocene depositional environments and coastal evolution of the Mekong River Delta, Southern Vietnam. Journal of Asian Earth Science .18 (2000) 427-439.

Nguyen, V. L., Ta, T. K. O., & Saito, Y. (2010). Early Holocene initiation of the Mekong River delta, Vietnam, and the response to Holocene sea-level changes detected from DT1 core analyses. Sedimentary Geology. https://doi.org/10.1016/j.sedgeo.2010.07.006

Nguyen, T. C., Schwarzer, K., & Ricklefs, K. (2023). Water-level changes and subsidence rates along the Saigon-Dong Nai River Estuary and the East Sea coastline of the Mekong Delta. Estuarine, Coastal and Shelf Science, 283, 108259. https://doi.org/10.1016/j.ecss.2023.108259

Nienhuis, J. H., Kim, W., Milne, G. A., Quock, M., Slangen, A. B. A., & Törnqvist, T. E. (2022). River Deltas and Sea-Level Rise. Annual Review of Earth and Planetary Sciences. https://doi.org/10.1146/annurev-earth-031621-093732

Proske, U., Hanebuth, T. J. J., Behling, H., Nguyen, V. L., Ta, T. K. O., & Diem, B. P. (2010). The palaeo-environmental development of the northeastern Vietnamese Mekong River Delta since the mid Holocene. The Holocene, 20(8), 1257–1268. https://doi.org/10.1177/0959683610374884

Proske, U., Hanebuth, T. J. J., Gröger, J., & Diem, B. P. (2011). Late Holocene sedimentary and environmental development of the northern Mekong River Delta, Vietnam. Quaternary International, 230, 57–66. https://doi.org/10.1016/j.quaint.2009.11.032

Renaud, F. G., Syvitski, J. P. M., Sebesvari, Z., Werners, S. E., Kremer, H., Kuenzer, C., Ramesh, R., Jeuken, A., & Friedrich, J. (2013). Tipping from the Holocene to the Anthropocene: How threatened are major world deltas? Environmental Sustainability. http://dx.doi.org/10.1016/j.cosust.2013.11.007

Salles, T., Mallard, C., Husson, L., Zahirovic, S., Sarr, A.-C., & Sepulchre, P. (2021). Quaternary landscape dynamics boosted species dispersal across Southeast Asia. Communications Earth & Environment, 2(240). https://doi.org/10.1038/s43247-021-00311-7

Sathiamurthy, E., & Voris, H. K. (2006). Maps of Holocene Sea Level Transgression and Submerged Lakes on the Sunda Shelf. The Natural History Journal of Chulalongkorn University.

Schimanski, A., & Stattegger, K. (2005). Deglacial and Holocene evolution of the Vietnam shelf: stratigraphy, sediments and sea-level change. Marine Geology. 10.1016/j.margeo.2004.11.001

Shepard, Donald. (1968). A two-dimensional interpolation function for irregularly-spaced data. Proceedings of the 1968 ACM National Conference. pp. 517-524. doi:10.1145/800186.810616.

Ta, T. K. O., Nguyen, V. L., Kobayashi, I., Tanabe, S., & Saito, Y. (2002). Holocene delta evolution and sediment discharge of the Mekong River, southern Vietnam. Quaternary Science Reviews. 21, 1807–1819.

Tanabe, S., Ta, T. K. O., Nguyen, V. L., Tateishi, M., Kobayashi, I., & Saito, Y. (2003). Delta evolution model inferred from the Holocene Mekong Delta, southern Vietnam. Society for Sedimentary Geology.76: P175–188. ISBN 1-56576-086-7.

Tamura, T., Saito, Y., Sieng, S., Ben, B., Kong, M., Sim, I., Choup, S., & Akiba, F. (2009). Initiation of the Mekong River delta at 8 ka: Evidence from the sedimentary succession in the Cambodian lowland. Quaternary Science Reviews, 28(3-4), 327–344. https://doi.org/10.1016/j.quascirev.2008.10.010

Tamura, T., Nguyen, V. L., Ta, T. K. O., Bateman, M. D., Gugliotta, M., Anthony, E. J., Nakashima, R., & Saito, Y. (2020). Long-term sediment decline causes ongoing shrinkage of the

Mekong megadelta Vietnam. Scientific Reports, 10(8085). https://doi.org/10.1038/s41598-020-64630-z

Tjallingii, R., Stattegger, K., Stocchi, P., Saito, Y., & Wetzel, A. (2014). Rapid flooding of the southern Vietnam shelf during the early to mid-Holocene. Journal of Quaternary Science, 29(6), 581-588. https://doi.org/10.1002/jqs.2731

Wang, Y., Zhang, B., Schoenbohm, L. M., Zhang, J., Zhou, R., Hou, J., & Ai, S. (2016). Late Cenozoic tectonic evolution of the Ailao Shan-Red River fault (SE Tibet): Implications for kinematic change during plateau growth. AGU Tectonics. 10.1002/2016TC004229

Wu, K., Liu, S., Shi, X., Colin, C., Zhang, H., Bassinot, F., Liu, Z., Fang, X., Miska, S., Nouet, J., Pinna-Jamme, R., Dapoigny, A., Mohamed, C. A. R., Khokiattiwong, S., & Kornkanitnan, N. (2023). The impact of changes in sea level and East Asian monsoon on sediment transport on the Sunda Shelf since the last deglaciation. Journal of Geophysical Research: Earth Surface, 128. https://doi.org/10.1029/2023JF007335

Zoccarato, C., Minderhoud, P. S. J., & Teatin, P. (2018). The role of sedimentation and natural compaction in a prograding delta: insights from the mega Mekong delta, Vietnam. Scientific Reports. 10.1038/s41598-018-29734-7

Zuo Xue, J. P. Liu, D. DeMaster, L. V. Nguyen, & T. K. O. Ta. (2009). Late Holocene Evolution of the Mekong Subaqueous Delta, Southern Vietnam. Marine Geology. https://doi.org/10.1016/j.margeo.2009.12.005

Tamura, T., Saito, Y., Nguyen, V. L., Ta, T. K. O., Bateman, M. D., Matsumoto, D., & Yamashita, S. (2012). Origin and evolution of interdistributary delta plains; insights from Mekong River delta. Geological Society of America. 4, P303-306. https://doi.org/10.1130/G32717.1

Li, L., Clift, P. D., & Nguyen, H. T. (2013). The sedimentary, magmatic and tectonic evolution of the southwestern South China Sea revealed by seismic stratigraphic analysis. Mar Geophys Res, 34, 341-365. https://doi.org/10.1007/s11001-013-9171-y

Book Chapter:

Carling, P. A. (2009). The Geology of the Lower Mekong River. In The Mekong. Chapter 2.P13-28.

Website:

Spatial analysis - interpolation. (2024). QGIS Documentation. https://docs.qgis.org/3.34/en/docs/gentle_gis_introduction/spatial_analysis_interpolation.html

Appendix

Appendix I: Excel file of raw core data

The following Excel file contains the values and calculations of all of the cores' sediment rate data. Excel file has been attached:

data collection

Appendix II: Excel file of rearranged data divided into 22 time slices

The following Excel file contains the available cores' sediment rate value before being used to generate interpolation within 500 years for 22 time slices. [Note:1) core 1-102 are used to assign artificial values on the boundary of the study area polygons as 0 to assure the precision of the interpolations; 2) 'total' column represents each core's total sediment deposition thickness in the entire Holocene period]

Excel file has been attached:

cumulative _sediment

Appendix III: Input interpolation rasters

The following package contains the corrected interpolation rasters (effect of sedimentation) before putting into the paleo-coastline model.

(corrected) 22_raster

Appendix IV: Corrected model landmass output

The following package contains the output of corrected landmass (accounts for sedimentation and sea-level changes) of the study area in 23 time slices. Sea-level curve changes and the sides effects on land as input which were also included in the package.

mekong_
correct

Appendix V: Original model landmass output

The following package contains the output of original landmass (accounts for only sea-level change) of the study area in 23 time slices.

mekong_
original